Science of the Total Environment 892 (2023) 164496

Contents lists available at ScienceDirect

Science of the Total Environment

journal homepage: www.elsevier.com/locate/scitotenv

Changes in air pollution, land surface temperature, and urban heat islands during the COVID-19 lockdown in three Chinese urban agglomerations

Zihao Feng, Xuhong Wang *, Jiaxin Yuan, Ying Zhang, Mengqianxi Yu

[a] College of Urban and Environmental Sciences, Northwest University, Xi'an 710127, China
[b] Shaanxi Key Laboratory of Earth Surface System and Environmental Carrying Capacity, Northwest University, Xi'an 710127, China
[c] Shaanxi Xi'an Urban Forest Ecosystem Research Station, Northwest University, Xi'an 710127, China

HIGHLIGHTS

- The COVID-19 lockdown reduced PM2.5 and NO2 by >14 % in all the three urban agglomerations.
- A sharp decrease (>25 %) occurred for $UHII_{night}$ in the three urban agglomerations during the COVID-19 lockdown.
- The reduction of $UHII_{night}$ is mainly due to reduced human activities and air pollutant emissions.
- Small-scale lockdowns do little to improve the environment.

GRAPHICAL ABSTRACT

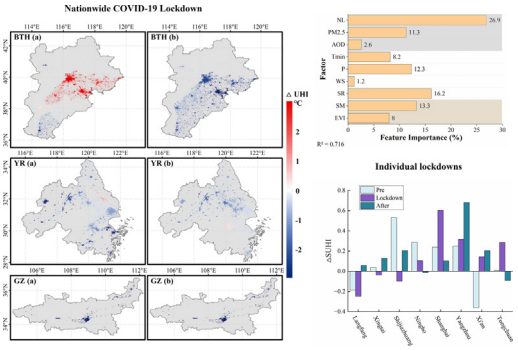

ARTICLE INFO

Editor: Shuqing Zhao

Keywords:
COVID-19 lockdown
Air pollution
Land surface temperature
Urban heat island
Aerosol
Urban agglomeration

ABSTRACT

COVID-19 has notably impacted the world economy and human activities. However, the strict urban lockdown policies implemented in various countries appear to have positively affected pollution and the thermal environment. In this study, Moderate Resolution Imaging Spectroradiometer (MODIS) land surface temperature (LST) and aerosol optical depth (AOD) data were selected, combined with Sentinel-5P images and meteorological elements, to analyze the changes and associations among air pollution, LST, and urban heat islands (UHIs) in three urban agglomerations in mainland China during the COVID-19 lockdown. The results showed that during the COVID-19 lockdown period (February 2020), the levels of the AOD and atmospheric pollutants (fine particles ($PM_{2.5}$), NO_2, and CO) significantly decreased. Among them, $PM_{2.5}$ and NO_2 decreased the most in all urban agglomerations, by >14 %. Notably, the continued improvement in air pollution attributed to China's strict control policies could lead to overestimation of the enhanced air quality during the lockdown. The surface temperature in all three urban agglomerations increased by >1 °C during the lockdown, which was mainly due to climate factors, but we also showed that the lockdown constrained positive LST anomalies. The decrease in the nighttime urban heat island intensity (UHIInight) in the three urban agglomerations was greater than that in the daytime quantity by >25 %. The reduction in surface UHIs at night was mainly due to the reduced human activities and air pollutant emissions. Although strict restrictions on human activities positively affected air pollution and UHIs, these changes were quickly reverted when lockdown policies were relaxed. Moreover, small-scale lockdowns contributed little to environmental improvement. Our results have implications for assessing the environmental benefits of city-scale lockdowns.

* Corresponding author at: College of Urban and Environmental Sciences, Northwest University, Xi'an 710127, China.
E-mail address: jqy_wxh@nwu.edu.cn (X. Wang).

http://dx.doi.org/10.1016/j.scitotenv.2023.164496
Received 9 March 2023; Received in revised form 7 May 2023; Accepted 25 May 2023
Available online 29 May 2023

1. Introduction

COVID-19, caused by severe acute respiratory syndrome coronavirus 2 (SARS-CoV-2), was characterized as a global pandemic by the World Health Organization (WHO) on 11 March 2020 (WHO, 2020) after its discovery in December 2019. By the end of November 2022, 637 million confirmed cases and 6.6 million deaths were reported globally (WHO, 2022). In response to this major public health emergency, national restrictions were adopted in >100 countries. The world economy has reportedly shrunk by 13–32 % due to the pandemic (Mousazadeh et al., 2021), and despite digital teaching efforts, >1 billion students did not receive normal education (Shulla et al., 2021). In addition, the restrictions on public transport, industrial production, human activities, and social distancing have led to global environmental changes (Lal et al., 2020), such as air pollution and urban thermal environmental changes (Cao et al., 2022; Chakraborty et al., 2021). This also provides the opportunity to study the environmental impacts of notable human interference.

The aerosol optical depth (AOD) is a proxy of the atmospheric pollution level, which measures the attenuation of light by suspended particles in the atmosphere (Xiang et al., 2022), and the AOD has been confirmed to decrease by 10 % due to the strict lockdown in 2020 (Fiedler et al., 2021). A significant decrease in the AOD during the COVID-19 lockdown was observed in North America and Europe (Parida et al., 2021a). Similarly, decreases in pollutant aerosols were detected in southwest (Chen et al., 2020) and eastern (Lin et al., 2021) China. In addition, air pollutant (PM_x, NO_x, CO, and SO_2) concentration anomalies were first observed due to the reduced human activities and factory emissions after the start of the COVID-19 lockdown (El Kenawy et al., 2021; Hu et al., 2021). Several studies have shown that the strict national lockdown policies have caused significant reductions in air pollutants worldwide (Bauwens et al., 2020; Yang et al., 2022a). During the worldwide urban lockdown, a significant decrease in the daily NO_2 concentration of 3–58 % was observed (Benchrif et al., 2021). Notable declines were widely observed in China (Agarwal et al., 2020), Pakistan (Ali et al., 2021), Germany (Cao et al., 2022), France (Kovács, 2022), Malaysia (Abdullah et al., 2020), Chile (Toro et al., 2021), and the USA (Bekbulat et al., 2021). Similarly, decreases in fine particles ($PM_{2.5}$) and CO were observed due to factory production and traffic restrictions (Alqasemi et al., 2021; Hidalgo García and Arco Díaz, 2022; Jamei et al., 2022). In contrast, the change in SO_2 was ambiguous (Hidalgo García and Arco Díaz, 2022; Tyagi et al., 2021), and even the opposite trend in O_3 was observed (Cao et al., 2022). However, the air quality in some economically underdeveloped areas has not been improved because of the COVID-19 lockdowns (Mandal et al., 2022; Martinez-Soto et al., 2021).

Changes in anthropogenic emissions and air pollutants can significantly affect the land surface temperature (LST) (Qian et al., 2022). Despite the decrease in the radiative forcing of aerosols during the global COVID-19 lockdown, the LST and air temperature did not show the expected rise and even decreased in Europe and North America (Parida et al., 2021a). Similar situations have also occurred in Iran (Roshan et al., 2021) and India (Parida et al., 2021b). This negative surface temperature anomaly can be partly explained by the evapotranspiration and cooling effects of the late harvest of crops (Chakraborty et al., 2021), but the reason for the reduction in the LST in urban areas with fewer crops remains unknown. However, the positive or negative changes in the LST in Chinese cities during the COVID-19 lockdown remain to be quantified and characterized.

Moreover, human heat emissions and air pollution decreased due to the significant reduction in human activities during the COVID-19 lockdown, which substantially impacted the urban heat island (UHI) phenomenon, a local climate change phenomenon in which the temperatures in urban areas are higher than those in rural surrounding areas owing to urbanization. Driving force analysis of the UHI phenomenon has shown that impermeable hardened surfaces (instead of permeable natural landscapes), background climate conditions and artificial heat emissions are major influencing factors (Oke, 1973). Among them, anthropogenic heat emissions, including the heat emissions originating from industrial plants, road transportation, commercial and industrial activities, domestic heating and cooling, space heating, human metabolism and vehicle exhaust, were the most sensitive major contributor to UHIs during the COVID-19 lockdown, and these heat emissions usually contribute 15–50 W/m^2 to the urban local heat balance (Sobrino et al., 2008). The linkage between lockdown measures and UHI variations can be quantified using in situ station monitoring and satellite temperature observations. Although we investigated the canopy heat island (CUHI) phenomenon, which is more essential than the surface urban heat island (SUHI) phenomenon for public health considerations (Oke et al., 2017), because the distribution of ground weather monitoring stations is sparse and susceptible to the surrounding conditions, it is difficult to obtain UHI information through actual in situ measurements. Satellite remote sensing data provide conditions for representing SUHIs due to their extensive coverage and high accuracy (Voogt and Oke, 2003). As a rapidly developing country, China now suffers from the heat island phenomenon, and the UHI problem has attracted increasing attention (Du et al., 2016; Wang et al., 2016). However, recent studies have noted that SUHIs were positively affected during the COVID-19 lockdown, namely, the strict human activity restrictions resulted in a significant decline in SUHIs in China (Cai et al., 2021). However, enhanced daytime surface urban heat islands ($SUHI_{day}$) due to the strict lockdown measures were also detected (Chakraborty et al., 2021). Although previous studies have analyzed the changes in SUHIs during the COVID-19 lockdown in China (Liu et al., 2022), the differences in SUHIs among urban agglomerations and the impacts of pollutant emissions and changes in human activities have not been explored.

As the first country to respond to the lockdown, the strict lockdown period varied from region to region in China. This provides sufficient evidence for the exploration of the differences between urban agglomerations under different COVID-19 lockdown states. Over time, small-scale lockdown policies (single or neighboring cities) were implemented, which also provides research support for the repeatability of the impacts of these lockdown measures. Therefore, three urban agglomerations with different lockdown times and development levels were selected in this study to address the following problems: (1) what are the impacts of the COVID-19 lockdown on air pollution, LST, and SUHIs? (2) Are there differences in the influences of the different urban agglomerations and lockdown levels on these three elements? (3) What are the changes caused by the strict lockdown measures that mainly affect SUHIs? Finally, this study could provide support for short-term air pollution control and thermal environment improvement policy formulation.

2. Materials and methods

2.1. Study area and time period

The differences of dry and wet regional background climatic conditions in different urban agglomerations, which are areas with strong human activities, serious air pollution and significant local climate of UHI, have been shown to significantly affect both the AOD and UHI (Ayanlade et al., 2019; Peng et al., 2011). Therefore, in this study, dry and wet zones were divided according to the isoprecipitation line (Fig. 1a). Among them, isoprecipitation line data were retrieved from the China Climate Zoning Map compiled by the China Meteorological Administration based on climate data from 1951 to 1970. According to the existing data quality and different dry–wet divisions, the Beijing-Tianjin-Hebei (BTH) and the Yangtze River Delta (YR) urban agglomerations were selected, ranking third and first, respectively, among all economic aggregates in China. Of these urban agglomerations, BTH is mainly distributed in a semi-humid region, while YR is distributed in a humid region. As the second largest urban agglomeration in western China, the Guanzhong (GZ) plain urban agglomeration is located in the same semi-humid region as the BTH urban agglomeration and was chosen as a comparative region due to the differences in the economic development level and COVID-19 lockdown time with the latter. Details of these urban agglomerations are shown in Text S1 & Table S1.

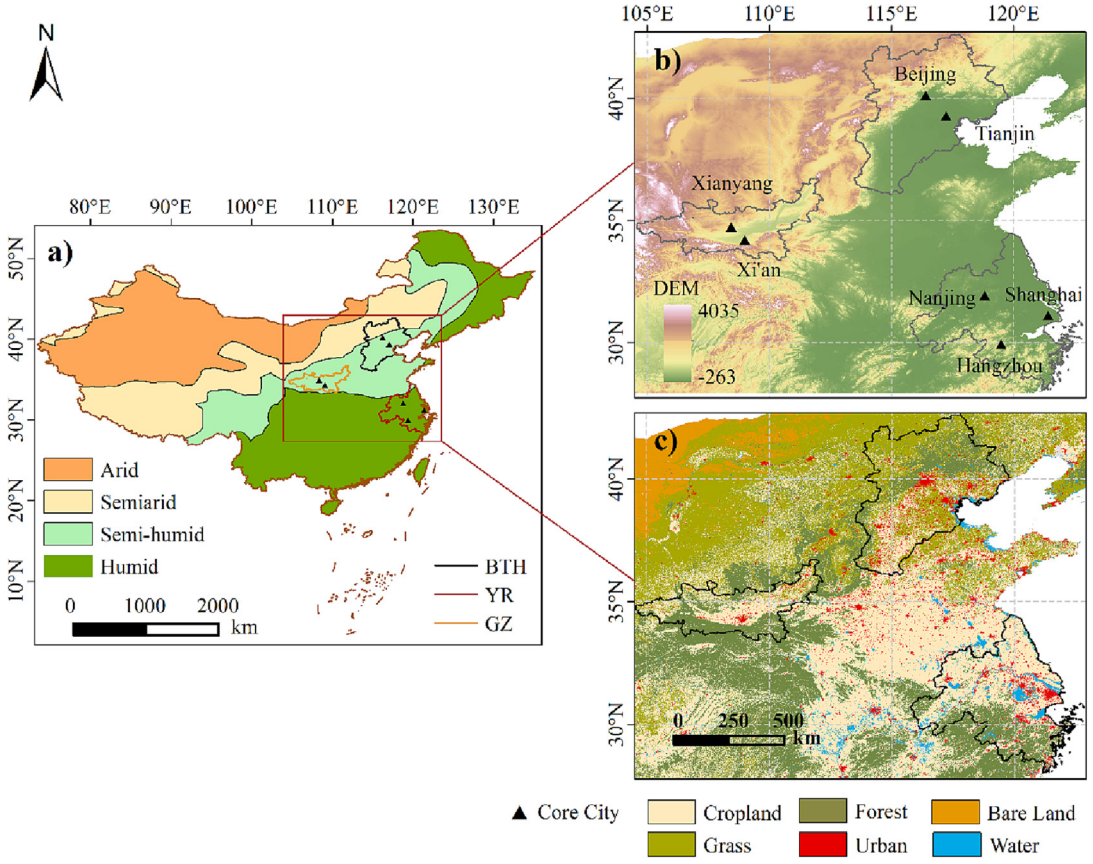

Fig. 1. Distributions of the three urban agglomerations, **a**) the wet–dry boundary, **b**) elevation and core cities, and **c**) the land cover type (obtained from the European Space Agency).

The dates of COVID-19 closures in the three urban agglomerations are provided in Table 1. The lockdown start time was identified as the start date of the first-level public health emergency response (factory shutdown, no gathering, and strict traffic control), and the end time coincided with a reduction in the response level. Human activity restrictions were initiated in all three city agglomerations at the end of January 2020, with those in YR and GZ continuing until the end of February, while the strict city lockdown in BTH continued until the end of April. Therefore, February 2020 was selected as the COVID-19 strict lockdown stage in this study, and January, March, and April were selected for comparative analysis.

2.2. Data sources

In this study, surface temperature data were obtained via satellite to study the impacts of the COVID-19 lockdown on the temperature and SUHIs. Similarly, satellite-obtained AOD, air pollutant, and nighttime light index data were combined with $PM_{2.5}$ and meteorological element product data to analyze the impacts of the lockdown measures on environmental and anthropogenic emissions. The peripheral 5*5 pixel mean was chosen to replace missing values, and the remaining vacant pixels were discarded to ensure the accuracy of the results. The details of data preprocessing are shown in the Supplementary File (Text S2). The data sources are presented in Table 2, with detailed data descriptions given in the following sections.

2.2.1. Air pollution data

Data on the AOD at 0.55 μm were obtained from the Google Earth Engine (GEE) database (MCD19A2 V6), a Moderate Resolution Imaging Spectroradiometer (MODIS) Terra and Aqua combined Multiangle Implementation of Atmospheric Correction (MAIAC) land AOD Level 2 product with a spatial resolution of 1 km (Lyapustin and Wang, 2018). The green band (0.55 μm) AOD over land was selected in this research. In this study, all daily AOD data in China were masked by the quality control band (AOD_QA), and pixels containing both clouds and surfaces covered with snow and ice were excluded. The AOD data in the GEE database were calculated as the monthly mean using a weighted average.

$PM_{2.5}$ data were obtained from Wei et al. (2021) using the Space-Time Extra-Trees (STET) model, exhibiting a high accuracy (R^2 = 0.86–0.90) and a spatial resolution of 1 km, and the data covered all of China. Furthermore, NO_2, CO, O_3, and SO_2 were obtained from the Sentinel-5P OFFL products in the GEE database (Copernicus/S5P/OFFL/L3). The Sentinel-5 precursor satellite was launched by the European Space Agency on 13

Table 1
Statistics on the COVID-19 lockdown dates in the three urban agglomerations.

Urban agglomeration	First-level public health emergency response		Source
	Active (level I)	Relief/level down	
BTH	January 25, 2020	April 30, 2020	http://www.hebei.gov.cn/
YR	January 25, 2020	February 24, 2020	http://www.jiangsu.gov.cn/
GZ	January 26, 2020	February 28, 2020	https://www.zj.gov.cn/ http://www.shaanxi.gov.cn/

Table 2.
Details of the data acquisition process in the three city agglomerations from January 2016 to June 2022.

Data	Resolutions	Source
Air pollution		
NO_2, CO, O_3, and SO_2 (Sentinel-5P offline)	Spatial: 1113.2 m Temporal: daily	https://s5phub.copernicus.eu
$PM_{2.5}$	Spatial: 1 km Temporal: monthly	Wei et al. (2021)
Aerosol optical depth (AOD) (MCD19A2 version 6)	Spatial: 1 km Temporal: daily Band: green band (0.55 μm)	Lyapustin and Wang (2018)
Meteorological elements		
Land surface temperature (LST) (Aqua MYD11A1 version 6.1) Daytime and nighttime LSTs	Spatial: 1 km Temporal: daily	Wan et al. (2021)
Maximum air temperature (T_{mx}), minimum air temperature (T_{mn}), precipitation (P), wind speed (WS), relative humidity (RH)	Spatial: 1 km Temporal: monthly	National Earth System Science Data Center, National Science & Technology Infrastructure of China (http://www.geodata.cn)
Surface conditions		
ERA5-Land Reanalysis Solar radiation (SR), soil moisture (SM)	Spatial: 0.1° × 0.1° Temporal: monthly	Copernicus Climate Change Service (C3S) Climate Data Store (CDS) (https://cds.climate.copernicus.eu/cdsapp#!/dataset/10.24381/cds.68d2bb30?tab=overview)
Enhanced vegetation index (EVI) (MOD13A2 version 6)	Spatial: 1 km Temporal: 16-day	Didan (2015)
Land cover classification	Spatial: 300 m Temporal: annual	ESA CCI (https://cds.climate.copernicus.eu)
Digital elevation model (DEM) (GTOPO30)	Spatial: 30 arc-seconds	U.S. Geological Survey (USGS) (http://www.webgis.com/terr_world.html)
Human activity		
Nighttime light (NL) (VIIRS monthly cloud-free DNB VCM)	Spatial: 463.83 m Temporal: monthly	Earth Observation Group (https://eogdata.mines.edu/products/vnl/)

October 2017 to monitor air pollution, and the data products could be openly accessed in September 2018. As offline (OFFL) data, the accuracy and coverage are better than those of near-real-time (NRTI) products, and quality control was completed. Considering the length of the product time series, we chose the daily Sentinel-5P OFFL products after January 2019, with a weighted average to the monthly sequence.

2.2.2. Meteorological elements

Daily surface temperature products were generated from Aqua MODIS-derived surface temperature products (MYD11A1, V6.1), as estimated by using the split-window algorithm (Wan, 2008). Daytime (LST_Day_1 km) and nighttime (LST_Night_1 km) LST data from January 2016 to June 2022 were obtained from the GEE database (Wan et al., 2021) (Table 2). The LST error was eliminated by the quality control (QC) band, and the monthly value was obtained via weighted averaging of the daily LST data form the GEE database.

The monthly maximum and minimum temperatures were spatially downscaled from the 30′ Climatic Research Unit (CRU) time series dataset with the WorldClim climatology dataset using delta spatial downscaling (Peng et al., 2019), with a spatial resolution of 1 km. The auxiliary data in this study were not involved in the calculation of UHIs. Precipitation, wind speed, and relative humidity data were all obtained from the downscaled ERA-5 dataset (Jing et al., 2016). The above types of data were validated against ground-station data, indicating a favorable consistency (Jing et al., 2016; Peng et al., 2019). The baseline climate conditions of the three urban agglomerations are shown in Figs. S3 and S4.

2.2.3. Nighttime light (NL)

Nighttime light data were obtained from the Earth Observation Group (EOG) database. These data are produced by the Day–Night Band (DNB) of the Visible Infrared Imager Radiometer Suite (VIIRS) of the Joint Polar-orbiting Satellite System (JPSS) (Elvidge et al., 2013). VIIRS cloud mask (VCM) products that completely excluded stray light were used in this study, and flares generated by gas combustion were eliminated (Elvidge et al., 2017). In this study, both air pollution and NL data were selected as representations of human activities.

2.3. Methods

2.3.1. Calculation method of the mean and percentage change

To assess the anomalies of each element during the COVID-19 lockdown, the difference between the 2020 (COVID-19 outbreak) and reference period (2016–2019) means was calculated as follows:

$$\Delta E = E(2020) - \overline{E}(2016 \sim 2019) \quad (1)$$

where ΔE is the anomaly of a given element during the lockdown, E (2020) is the mean over the strict restriction period in 2020 (January to April), and (2016–2019) is the mean of the same months during the reference period. Thus, the change in the element percentage can be derived as follows:

$$\Delta E = \Delta E / \overline{E}(2016 \sim 2019) \times 100\% \quad (2)$$

where ΔE is derived from Eq. (1).

2.3.2. Urban/rural division and SUHI calculation

In this study, the simplified urban-extent (SUE) algorithm was used to define urban–rural ranges (Chakraborty and Lee, 2019). The main steps are as follows:

1) According to the digital elevation model and land cover classification products, combined with the municipal administrative boundaries of China (https://www.resdc.cn), urban and built-up pixels exceeding the median elevation of ±50 m were removed.
2) Urban and built-up pixels within the reserved areas of all boroughs were identified as urban areas.
3) The other pixels within the administrative boundaries (excluding water bodies, ice and snow, and forest pixels) were identified as rural areas.

Urban–rural division details are shown in Fig. S1. The urban–rural boundary derived by the SUE algorithm can reduce the UHI anomalies caused by buffer size differences, and the reliability has been verified (Liu et al., 2022).

Based on the divided urban and rural areas and LST data, the SUHII can be determined as follows:

$$SUHII = \overline{LST}_{Urban} - \overline{LST}_{Rural} \quad (3)$$

where and are the mean urban and rural LSTs, respectively, during the study period. The difference in the intensity of the SUHI between the COVID-19 lockdown and reference periods can be obtained with Eq. (1).

3. Results

3.1. Changes in the AOD and air quality during the lockdown

The AOD showed significant differences among the three urban agglomerations in February 2020 relative to the reference period (Fig. 2). Both GZ and YR exhibited high proportions of negative anomalies, at 88.35 % and 93.54 %, respectively (Table 3). In contrast, BTH showed a positive mean change in the area of 74.48 %, and the AOD mean increased by 0.09. In March, the number of pixels indicating negative anomalies in BTH and YR increased, and a significant decrease signal (BTH: −0.12; YR: −0.18) of the AOD mean was observed. There was a positive anomaly in central GZ during the same period (44.79 %), which also led to a slight increase in the overall average AOD (+0.01).

It has been shown that $PM_{2.5}$ is highly correlated with the AOD (Chu, 2006; Yang et al., 2022b), and the distributions of the $PM_{2.5}$ anomalies in BTH and YR has some similarity to AOD (Fig. 2). However, the decreasing amplitude and pixel proportion of $PM_{2.5}$ in the two urban agglomerations were higher than those of the AOD (Table 3), which may suggest that the effect of the lockdown on $PM_{2.5}$ was greater than that on the AOD. In contrast, the negative $PM_{2.5}$ anomaly in GZ during the lockdown period was not closely associated with the change in the AOD. This inconsistency may be related to the frequent sand and dust weather conditions in GZ (You et al., 2015). Dusty weather can lead to a higher proportion of respirable particles (PM10) than that of $PM_{2.5}$ (Neff et al., 2013), resulting in a positive AOD anomaly not driven by $PM_{2.5}$.

The negative AOD and $PM_{2.5}$ anomalies in 2020 (February and March) with respect to the 2016–2019 mean exhibited similar distributions (Fig. 2). However, the interannual mean change in each urban agglomeration was notable. Despite certain interannual fluctuations, the highest negative $PM_{2.5}$ anomaly was observed during the strict lockdown period (February 2020) relative to 2016–2019 (Fig. 2, line chart), and the AOD also showed similar changes. The reductions in human activities and emissions caused by the COVID-19 lockdown may have contributed to this phenomenon (Parida et al., 2021a). However, in March, when the lockdown policies in YR and GZ were relaxed (Table 1), negative AOD and $PM_{2.5}$ anomalies were still observed in these two urban agglomerations relative to 2019. Therefore, the interannual AOD and $PM_{2.5}$ changes in January

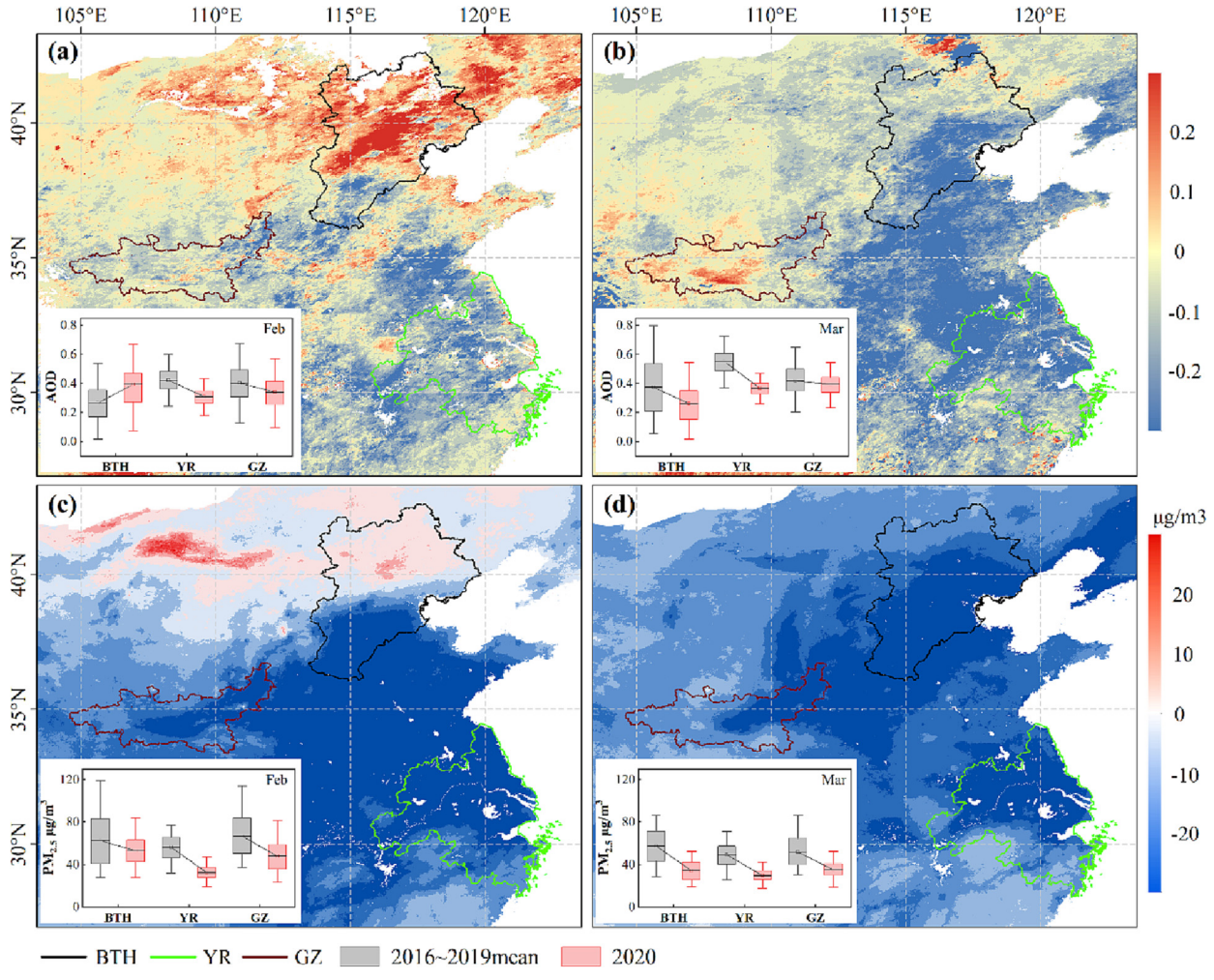

Fig. 2. AOD (a Feb., b Mar.) and $PM_{2.5}$ (c Feb, d Mar) anomalies in 2020 compared to the 2016–2019 mean in the urban agglomerations during the effective lockdown period (The box plot shows the change in the average AOD & $PM_{2.5}$ in the three urban agglomerations).

Table 3
AOD anomalies and percentages of pixels with different trends (up and down) in 2020 relative to the 2016–2019 mean. * indicates passing the $p < 0.05$ significance test.

Urban agglomeration (month)	AOD			$PM_{2.5}$		
	Anomaly & change %	Up (%)	Down (%)	Anomaly & change %	Up (%)	Down (%)
BTH (Feb.)	+0.09* (+32.61 %)	74.48	25.52	−9.28* (−14.89 %)	37.97	62.03
YR (Feb.)	−0.11* (−28.07 %)	6.46	93.54	−23.69* (−42.20 %)	0	100
GZ (Feb.)	−0.05* (−15.15 %)	11.65	88.35	−18.70* (−28.08 %)	0	100
BTH (Mar.)	−0.12 * (−31.38 %)	5.26	94.74	−23.07* (−40.25 %)	0	100
YR (Mar.)	−0.18 * (−33.19 %)	17.22	98.28	−19.24* (−39.21 %)	0	100
GZ (Mar.)	−0.01 (−2.41 %)	44.79	55.21	−16.59* (−32.15 %)	0	100

and April were considered (Fig. S5). In the three urban agglomerations, obvious and persistent negative $PM_{2.5}$ anomalies occurred in January and April from 2016 to 2020, which may be related to the strict air pollution control measures introduced by China in 2013 (Zhou et al., 2022). The factors impacting the AOD are complex, and in addition to the possible effects of human activities, positive precipitation and relative humidity anomalies can affect AOD changes (Fig. 4). This leads to complex interannual fluctuations in the AOD and anomaly distributions that differ from those of $PM_{2.5}$.

Compared to 2019, negative NO_2 and CO anomalies were observed in the three urban agglomerations in February 2020 (Fig. 3). Among them, the negative average percentage of NO_2 changed significantly, at >25 % in all urban agglomerations (Table S2). However, this phenomenon did not last until March 2020 (policy easing), and although it still declined from the 2019 level, the magnitude was reduced. The source of NO_2 is mainly a high-temperature combustion process (motor vehicle exhaust, engineering boilers, etc.). The COVID-19 lockdown (level I), resulting in a large number of factory shutdowns and motor vehicle bans (Wang and Su, 2020), was the main reason for the decline in NO_2 in February 2020. For the same reason, negative CO anomalies also occurred in the three urban agglomerations, namely, −8.97 % (BTH), −4.25 % (YR) and −10.54 % (GZ). Both the negative NO_2 and CO anomalies declined in March, which could be attributed to the increased emissions due to policy easing. During the COVID-19 lockdown, the O_3 anomalies were the opposite to those of the other pollutants. The main reason was the sharp decline in NO_2, which exceeded the volatile organic compound (VOC) concentration (Li et al., 2020), resulting in a decline in the titration effect on O_3. The distribution of SO_2 anomalies in February 2020 exhibited obvious north–south differences. A significant drop in SO_2 during the lockdown was observed in YR, consistent with the findings of several studies (Hu et al., 2021; Li et al., 2020; Wu et al., 2021), due to the reduction in factory and automobile activities. The increase in SO_2 in the northern urban agglomerations may be due to the low wind speed and high relative humidity (Zhao et al., 2020). Overall, during the strict lockdown period (February), the concentrations of several air pollutants were significantly affected by the reduced human activities. However, this influence state did not last after policy relaxation.

3.2. Changes in the LST and meteorological elements during the lockdown

According to the difference in lockdown policies, the study period was divided into February and March to compare the LST under different lockdown levels. The spatial distributions of the nighttime and daytime LST anomalies (°C) in the three urban agglomerations during the lockdown period in 2020 (1 February–31 March) with respect to the 2016–2019 mean are shown in Fig. 5. The LST (daytime) in February 2020 in the three urban agglomerations increased by 1.04 °C (BTH), 1.97 °C (YR) and 3.27 °C (GZ) relative to the reference data (2016–2019). Notably, severe negative (over −5 °C) LST anomalies occurred in the middle of the BTH (Fig. 5a). Similar to the daytime LST, the nighttime LST in February was dominated by positive anomalies. Both BTH and GZ exhibited >3 °C of warming, while in 12 % of the area of YR, negative anomalies were observed (Fig. 5b). Negative LST (daytime) anomalies in March covered the central part of GZ, the northern part of YR, and most of BTH. Only BTH showed a lower average LST (daytime) among the three urban groups than that over the past four years. The nighttime LST anomalies were not obvious in March (changes <1 °C). The southern part of BTH and the northern part of GZ showed negative changes, while the other areas mostly exhibited positive anomalies.

To analyze the air temperature during the day and at night, T_{mx} and T_{mn} were selected in this study. As the meteorological elements are closely related to the LST (Benali et al., 2012), the air temperature anomalies exhibited a similar distribution to that of the LST anomalies (Fig. 4; T_{mx} and T_{mn}

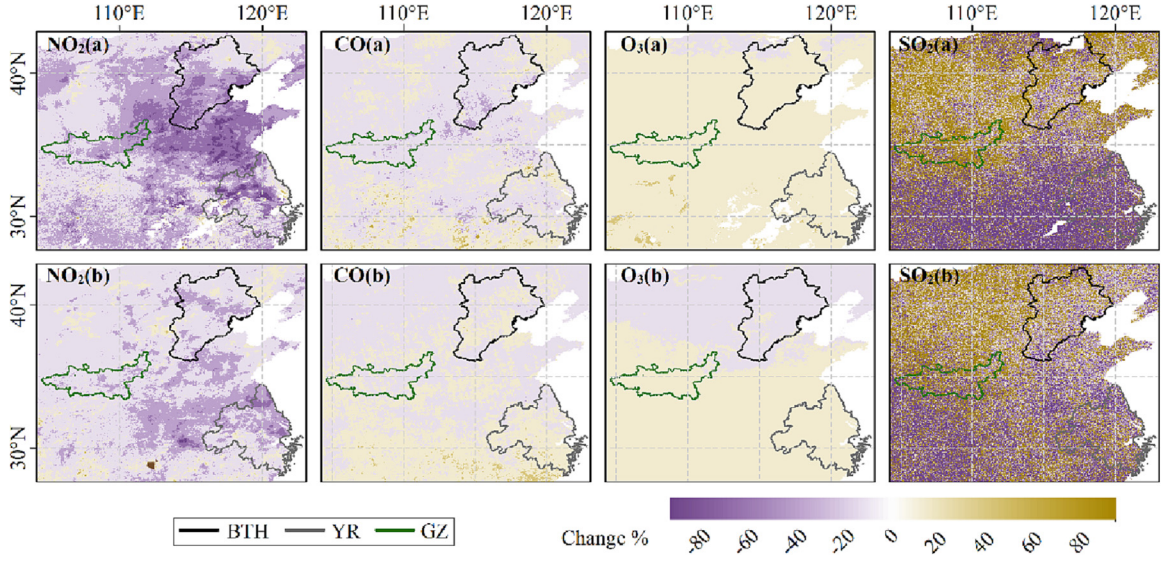

Fig. 3. Distribution of the atmospheric pollutant anomalies between 2020 and 2019 (a Feb., b Mar.) based on Sentinel-5P data.

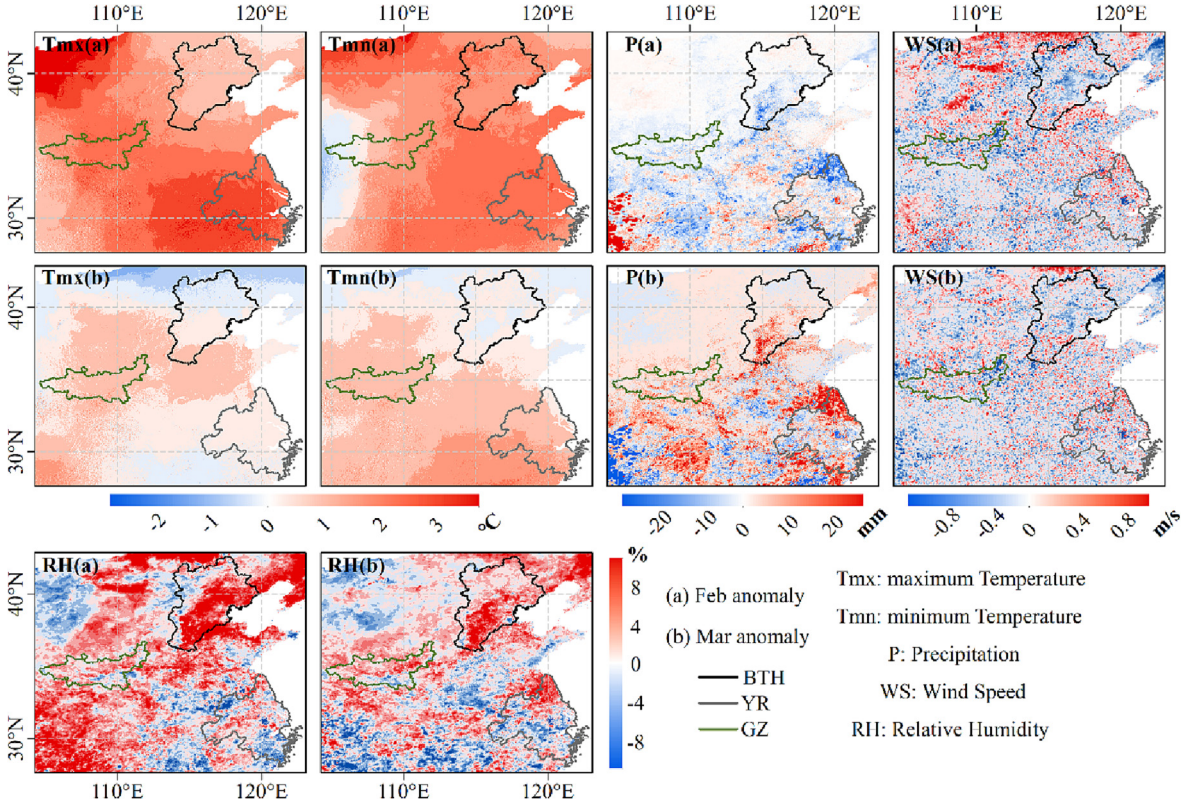

Fig. 4. Meteorological element anomalies in 2020 with respect to the 2016–2019 mean in BTH, YR, and GZ from 1 February–31 March (**a** February, **b** March).

(a)). During the day and at night in February 2020, relative to 2016–2019, positive temperature anomalies were observed in all three urban agglomerations. However, in contrast to the LST, the highest positive temperature anomalies occurred in YR. In addition to the difference in influencing factors between LST and air temperature, the difference in daily data collection time may also be the cause of this phenomenon. The daily transit time of AQUA satellites is fixed at 1.30 AM and 1.30 PM, and T_{mx} and T_{mn} are not guaranteed to synchronize with this time (Wan et al., 2021). In March, the temperature and LST consistently changed in BTH and YR. However, the negative LST anomalies in GZ exhibited the opposite trend to the temperature change.

Precipitation and relative humidity can negatively affect the LST. The thick cloud clusters during precipitation events and the high humidity levels before and after rainfall are important factors hindering thermal radiation surface absorption (Du et al., 2016). In February, the central part of the BTH showed a slight increase in precipitation, while the relative humidity exhibited a severe positive anomaly from the reference data (2016–2019). Moreover, the positive anomalies of these two meteorological elements in the middle of GZ and the northern YR part in March corresponded to the decrease in the LST. Strong winds help dilute and spread aerosols (Cugerone et al., 2018), allowing more radiant energy to reach the surface. Therefore, the wind speed anomaly distribution was similar to the LST anomaly distribution (Fig. 4; WS).

3.3. SUHI anomalies caused by the COVID-19 lockdown

The UHII anomalies in each city within the three urban agglomerations during the strict COVID-19 lockdown period (February 2020) relative to the 2016–2019 mean are shown in Fig. 6. The daytime SUHIs in YR and GZ in February 2020 were significantly lower than those over the past four years, decreasing by 2.48 and 1.01, respectively, and over 90 % of the cities exhibited negative anomalies. This phenomenon could presumably be attributed to the reduction in anthropogenic heat emissions. Although the reduction in pollution could increase the solar radiation absorbed by the surface, it exerted a certain promotion effect on SUHIs (Jin et al., 2010). However, this effect could not offset the negative SUHI anomalies caused by the reduction in anthropogenic heat emissions. Compared to those in GZ and YR, during the strict lockdown phase, the daytime SUHI changes in the central cities of BTH could not be explained. Despite the significant drop in human activities (Fig. S6), the SUHIs in the central cities of BTH showed positive anomalies. At the same time, the AOD and $PM_{2.5}$ in this area showed increasing trends (Fig. 2), which could not explain the positive SUHI anomalies. After studying the changes in the surface temperatures in the urban and rural areas (Table S3), an anomaly was discovered. Compared to that during the past four years, the urban surface temperature did not significantly change during the COVID-19 lockdown, while the rural surface temperature sharply decreased. This phenomenon may be due to the delay in winter crop harvesting during the lockdown, which caused significant cooling in rural areas through evapotranspiration (Chakraborty et al., 2021), leading to larger urban–rural temperature differences.

All three urban agglomerations showed significant downward trends in nighttime SUHIs in 2020 February relative to 2016–2019, with >95 % of the cities showing a decline (Fig. 7). Among them, the negative SUHI anomaly in GZ was the largest (−2.25), followed by those in BTH and YR, at −1.72 and −0.64, respectively. Significant reductions in human activities (Fig. S6) and air pollution (Figs. 2 and 3) may have contributed to the decline in SUHIs. The human activities of daily life emit large amounts of heat, soot, and greenhouse gases into the atmosphere. First, the atmosphere is directly affected by anthropogenic waste heat, causing the temperature to rise with corresponding feedback to the land surface (Du et al., 2016); second, dust and greenhouse gases cover urban areas, resulting in increased surface longwave radiation absorption (Arnfield, 2003).

During the city lockdown relaxation phase, the nighttime SUHIs in all cities of BTH decreased relative to the 2016–2019 mean (Fig. S7), but the decrease was only 0.21 (Fig. 7). Contrary to BTH, the daytime and nighttime SUHIs in YR and GZ mostly showed positive anomalies, which were 0.17 and 0.15 higher, respectively, than the average value over the past

four years. With the relaxation of the epidemic prevention policies (Table 1), the increase in human activities positively impacted the SUHI phenomenon (Peng et al., 2011). It should be noted that before the COVID-19 lockdown policy was relaxed, BTH still showed a small positive NL anomaly in March (Fig. S6), and similar anomalies also occurred in Wuhan (Deng et al., 2022), which may be related to the resumption of the production activities of key factories in early March and the return to work of nonlocal personnel.

Before and after the strict city lockdown, the daytime and nighttime SUHIs in the three urban agglomerations did not show the same negative anomalies as those observed in February 2020 (Fig. S7). This indicates that the impact of the COVID-19 lockdown on SUHIs only lasted for a month and soon disappeared after the restrictions on human movement were lifted. Furthermore, the ΔSUHI values of the core cities and other cities in the three urban agglomerations during the COVID-19 lockdown are shown in Table S4. The ΔSUHI value of the core cities at night in February 2020 was not significantly higher than that of the other cities. However, in March 2020, this balance was upset. The drop in SUHIs at night in Beijing and Tianjin was significantly greater than that in the other cities (over 65 %), indicating that the lockdown exerted a more pronounced impact on these two megacities. As the core cities in BTH, a high COVID-19 lockdown level was also maintained in these two cities in March, which may be the reason for the negative SUHI anomalies. The opposite was observed in GZ, where the SUHIs in the core cities increased more significantly than those in the other cities after lockdown policy easing, which is due to the more rapid urban development in the core cities in recent years (http://www.shaanxi.gov.cn/).

4. Discussion

4.1. Impact of the COVID-19 lockdown measures on the air quality

The reductions in human activities and dust emissions caused by the COVID-19 lockdown have significantly improved the global atmospheric environment (Lal et al., 2020). Under these restrictive measures, the AOD, $PM_{2.5}$, NO_2, and CO levels decreased during the lockdown in the three urban agglomerations (Figs. 2 and 3). However, the SO_2 and O_3 levels did not significantly improve. Similar results were also obtained by Cao et al. (2022) and Agarwal et al. (2020). In this study, negative AOD and $PM_{2.5}$ anomalies occurred in February 2020 relative to 2019. Short-term climate change may have contributed to the decline (Fig. S8). Although AOD has a strong correlation with $PM_{2.5}$, as a product describing the light reduction of aerosol, AOD is also significantly affected by other natural factors, such as air humidity, except by particulate matter. This property also leads to the failure to fully match the changing trend of AOD and $PM_{2.5}$ (Fig. S5). However, the long-term trend shows that $PM_{2.5}$ reduction occurs not only during this period but also before and after the COVID-19 lockdown (Fig. S5). Moreover, this downward trend has continued since 2016 (Fig. 2). The reason for this continuous reduction in pollution is the implementation of strict pollution control policies in China since 2013 (https://www.gov.cn/). With the elimination of high-energy-consumption and high-pollution industries and the designation of stricter corporate sewage standards, environmental pollution has been significantly improved. Persistent improvements in air pollution may lead to overestimation of the impact of the COVID-19 lockdown on the atmospheric environment.

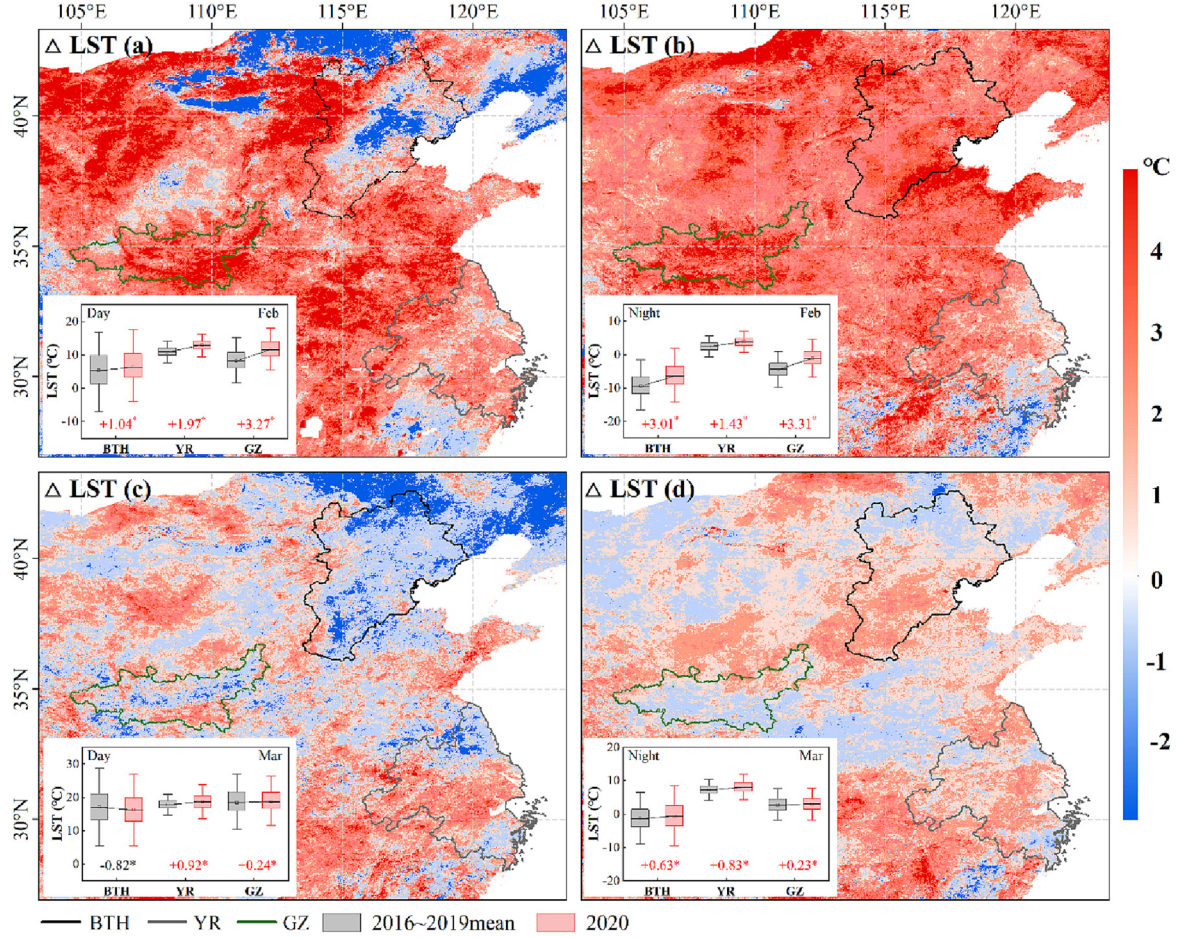

Fig. 5. Daytime and nighttime LST anomalies (°C) in 2020 with respect to the 2016–2019 mean in BTH, YR, and GZ from 1 February–31 March (**a** Feb. daytime, **b** Feb. nighttime, **c** Mar. daytime, **d** Mar. nighttime). The box plot shows the change in the average LST in the three urban agglomerations and * indicates passing the $p < 0.05$ significance test.

Therefore, after simple linear fitting of the $PM_{2.5}$ concentrations in the three urban agglomerations in recent years, $PM_{2.5}$ anomalies likely caused by city closure in February 2020 were confirmed based on the predicted values: $-1.04\ \mu g/m^3$ (BTH), $-18.61\ \mu g/m^3$ (YR), and $-7.27\ \mu g/m^3$ (GZ). Therefore, this has at least led to an overestimation of >10 % of the pollution improvements in these urban agglomerations. The strict restrictions have indeed significantly improved air pollution, but the rebound after policy relaxation was also very rapid, especially for NO_2 and CO (Fig. 3b). This requires policymakers to carefully consider human activity constraints when formulating policies.

4.2. Impact of the COVID-19 lockdown measures on the LST

The COVID-19 pandemic has exerted a life-changing shock on society and has led to sweeping urban lockdowns in >100 countries. As a result, there were significant reductions in human activities worldwide during the lockdown (Ali et al., 2021; Cai et al., 2021), which may impact the climate. Much of the discussion regarding the climate impact of the COVID-19 lockdown has focused on the temperature. Much research and evidence have indicated that the strict travel restrictions have led to a significant drop in the surface and air temperatures (Pal et al., 2022; Parida et al., 2021a). However, this is contrary to the results in this study since almost all cities in the three urban agglomerations exhibited positive LST anomalies during the lockdown (Fig. 5). Similar results were also obtained in East Java, India (Purwanto et al., 2022).

In this study, the LST and air temperature in the three urban agglomerations showed upward trends during the lockdown period relative to the 2016–2019 average. Only the central part of BTH exhibited negative daytime LST anomalies (Fig. 5), which were mainly distributed in rural pixels (Table S3). Therefore, there is insufficient evidence to verify that China's lockdown due to the COVID-19 epidemic has negatively impacted the LST. The precipitation and relative humidity in the three urban agglomerations increased, and the wind speed decreased. These are all related factors that may induce a temperature drop. According to the correlation heatmap (Fig. S8), the change in the LST during the lockdown was not only associated with air temperature variation but also correlated with the RH to a high degree. This is caused by the radiation obstruction effect of water vapor during the day and the thermal insulation effect at night (Wang et al., 2016). In contrast, T_{mx} did not show a significant correlation with RH and P, so LSTD had a more pronounced downward trend when the two factors rose significantly, which also explained the unusual difference between February LST and T_{mx} in the middle of BTH (Figs. 4 & 5). Similarly, the difference in the influence of each element on LSTN and T_{mn}, as well as the gap in recording time, may lead to a certain negative correlation between them. In addition, a nonsignificant negative correlation appeared between the LSTD and AOD. Smaller aerosol optical thicknesses characterize lower radiative forcing, which may impose some positive effect on the daytime LST.

We could speculate that the different response times of countries to the COVID-19 epidemic may be the reason for the difference in the obtained conclusions. China's strict lockdown began at the end of January 2020, while most other countries started human movement restrictions after mid-March (Ali et al., 2021; Cao et al., 2022; Parida et al., 2021a). This results in different seasonal conditions and atmospheric circulation factors. During the strict city closure period in China, the LST was mainly affected by the rising background temperature and exhibited a positive anomaly

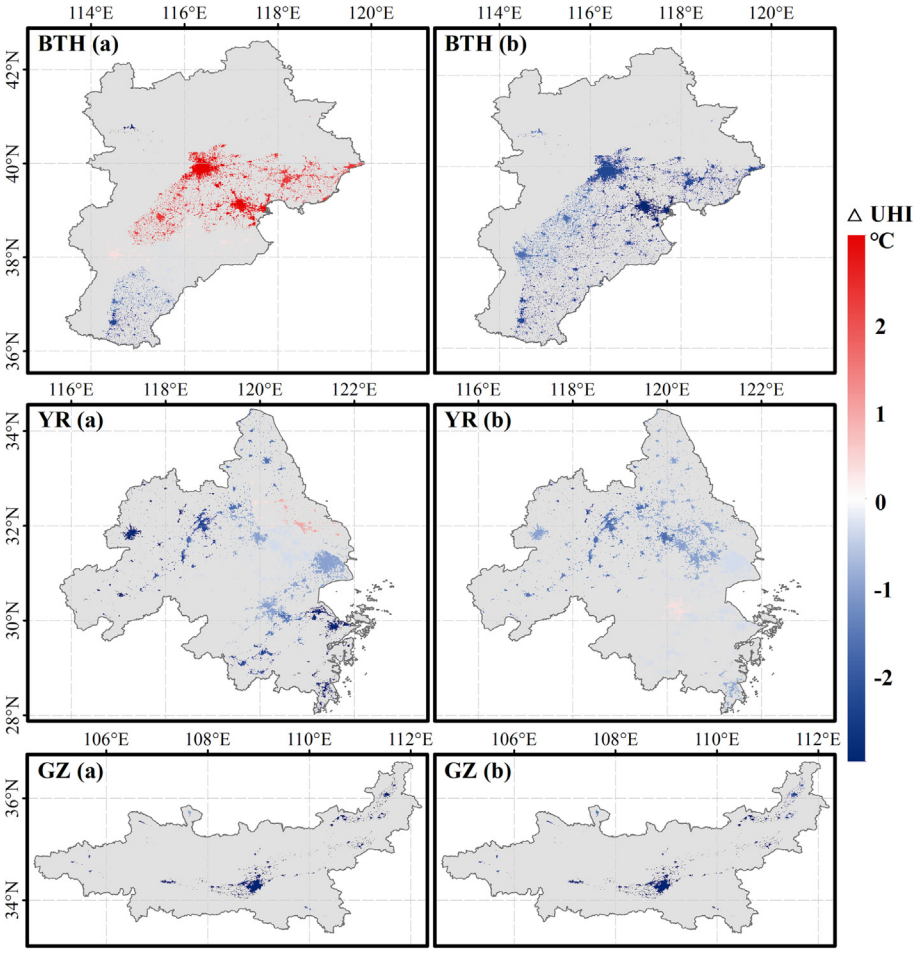

Fig. 6. Three urban agglomerations: (**a**) Daytime and (**b**) nighttime surface urban heat island anomalies in the urban areas (divided by the SUE algorithm) during the 2020 lockdown with respect to the 2016–2019 mean.

(Text S4). However, the COVID-19 lockdown has resulted in reductions in human activities and heat emissions, restricting the rise in the LST. This has led to a significantly smaller increase in the LST in urban areas than in rural areas (Table S5). Therefore, the COVID-19 lockdown may not be the main factor leading to the decline in the LST, but it imposed a clear inhibitory effect on the positive LST anomalies in cities.

4.3. Impact of the COVID-19 lockdown measures on SUHIs

During the strict COVID-19 lockdown, the SUHIs in the three urban agglomerations significantly dropped (Fig. 6), and similar negative anomalies were widely distributed worldwide (Ali et al., 2021; Liu et al., 2022; Parida et al., 2021a). In this study, we showed that the COVID-19 lockdowns severely reduced human activities and heat emissions (Fig. S6). To explore the causes of the changes in SUHIs during the lockdown period, random forest regression was applied to each city to examine the impacts of the changes in human activities and climate and surface conditions on the nighttime SUHIs (the influencing factors of daytime SUHIs are very complex (Liu et al., 2022) and have not been studied). Due to a similar mechanism to precipitation, the relative humidity was not considered. The results showed that NL, which characterizes human activities, attained the highest importance, and $PM_{2.5}$ also ranked high (Fig. 8). This verifies that the reductions in human activities and emissions caused by the COVID-19 lockdown are an important reason for the observed changes in SUHIs. Similar conclusions were also given by Liu et al. (2022) and Shikwambana et al. (2021). In addition, changes in solar radiation and soil moisture play a nonnegligible role in SUHI reduction.

The COVID-19 lockdown effectively alleviated SUHIs, which is likely a promising measure for policymakers to remediate the urban thermal environment. However, it should be noted that the SUHIs in all urban agglomerations exhibited rapid rebounds upon lockdown policy easing (Fig. 7). The same SUHI trend also occurred in Pakistan (Ali et al., 2021). It is obvious that the changes due to the COVID-19 lockdown in the urban thermal environment were short-lived. This leads to the following important question: will SUHIs always decline due to the implementation of strict

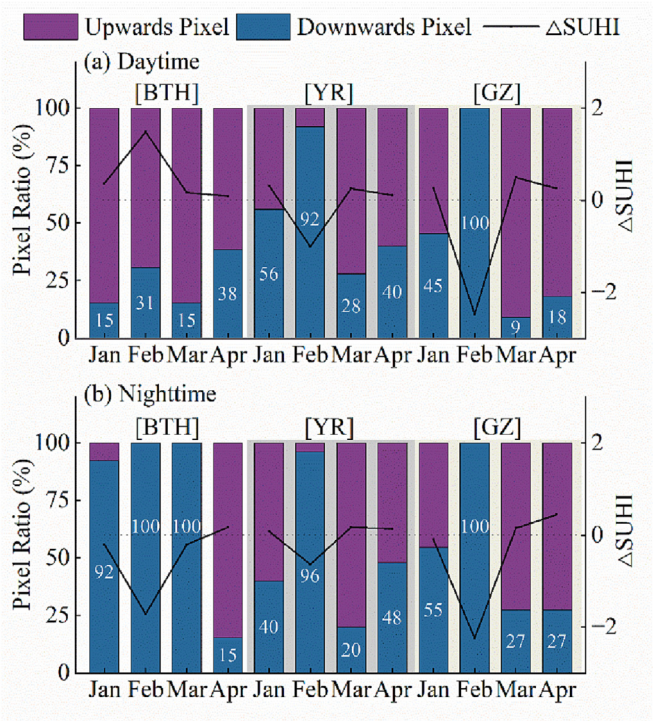

Fig. 7. Percentages of upward and downward pixels (histogram) and changes (line) in the SUHI intensity (SUHII) in the three urban agglomerations from January 1–April 31, 2020 with respect to the 2016–2019 mean (**a** daytime, **b** nighttime).

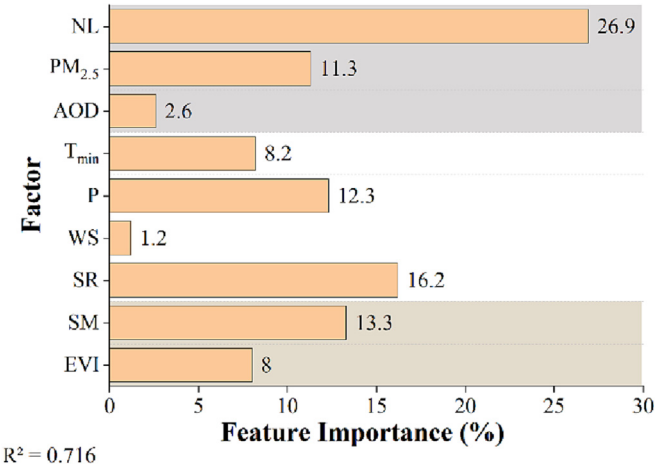

Fig. 8. Feature importance of the influencing factors of the nighttime SUHIs in the three urban agglomerations obtained via random forest regression (nighttime light (NL), $PM_{2.5}$, and AOD are used to characterize the changes in human activities and heat emissions. The minimum temperature (T_{mn}), precipitation (P), wind speed (WS), and solar radiation (SR) represent climate change. Soil moisture (SM) and the enhanced vegetation index (EVI) are used to characterize surface conditions).

lockdown measures? To explore this issue, eight cities with a second lockdown period were selected (Table S6). To eliminate the impact of strict city closure, the mean SUHIs over the last four years except 2020 were selected for comparison (Fig. 9). The results were unexpected: in contrast to during the strict lockdown period in February 2020, five cities did not experience a reduction in SUHIs during their individual lockdowns. The three cities with declines in SUHIs were all distributed in the BTH urban agglomeration. An interesting phenomenon is that the three cities with decreasing SUHI trends are adjacent and experienced the same lockdown times. After the first large-scale lockdown, China began to implement refined COVID-19 prevention and control measures, i.e., epidemic risk areas were more accurately delineated (http://www.nhc.gov.cn/). This ensured the necessary production and life activities to a certain extent, resulting in nonsignificant changes in SUHIs. In addition, due to heat exchange between neighboring cities, lockdown policy implementation in adjacent cities can only impose favorable inhibitory effects on SUHIs. This shows that the notable negative SUHI anomalies caused by the strict lockdown in 2020 may be difficult to replicate. Therefore, activity restrictions should be carefully considered when specifying policies to manage the urban thermal environment.

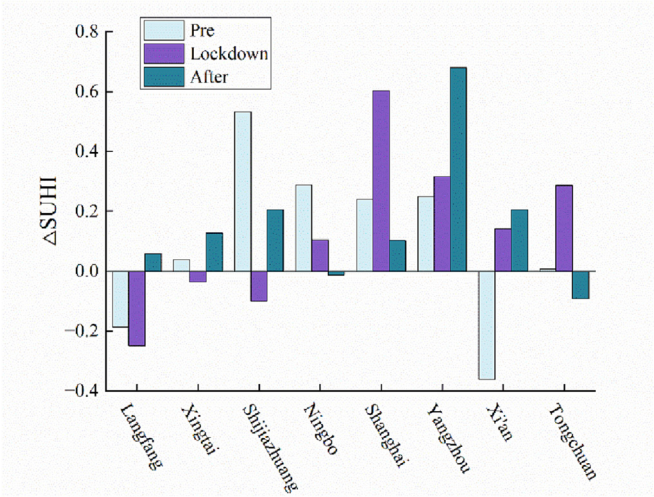

Fig. 9. Nighttime SUHI anomalies (°C) before, during, and after individual lockdowns with respect to the recent four-year mean in eight cities (as a comparison, the length of time before and after each city lockdown is one month).

5. Conclusion

The COVID-19 lockdown has greatly affected people's lives and the urban environment. During the most stringent Level I response period, the air pollutants $PM_{2.5}$ and NO_2 significantly decreased in all three urban agglomerations, exceeding 14 %. In addition, SUHIs significantly decreased (>25 %) during the lockdown period regardless of the climate conditions and economic level. The negative SUHI anomalies were mainly due to the reduced human activities and heat emissions. However, rapid SUHI rebound occurred after lockdown policy easing. When travel restrictions are not adopted in neighboring cities, the SUHI suppression effect of the lockdown may be offset by intercity heat exchange.

In this study, we found that if background climate variations or long-term trend rates are ignored, the impact of the COVID-19 lockdown may be miscalculated. Therefore, the identification of long-term trend changes and anomalies is very important for the study of city closure impacts.

Our findings suggest that human behavior-based policies can directly, immediately and significantly affect the reduction and recovery of air pollution levels and SUHIs. However, these impacts are temporary and require intercity alliances in terms of policy formulation to achieve effective and sustained urban environmental improvements.

CRediT authorship contribution statement

Zihao Feng: Data curation, Writing – original draft. **Xuhong Wang:** Conceptualization, Writing – review & editing. **Jiaxin Yuan:** Visualization, Investigation. **Ying Zhang:** Data analysis. **Mengqianxi Yu:** Methodology.

Data availability

Data will be made available on request.

Declaration of competing interest

The authors declare that they have no known competing financial interests or personal relationships that could have appeared to influence the work reported in this paper.

Acknowledgment

The authors are indebted to European Space Agency for archiving the land cover and Sentinel-5P datasets, National Earth System Science Data Center for archiving Meteorological datasets, NASA for archiving MODIS datasets, Earth Observation Group for archiving nighttime light datasets, U.S. Geological Survey for archiving digital elevation model and the World Health Organization (WHO) for the infected case report globally. The authors acknowledge the financial support provided by The National Natural Science Foundation of China (41971387).

Appendix A. Supplementary data

Supplementary data to this article can be found online at https://doi.org/10.1016/j.scitotenv.2023.164496.

References

Abdullah, S., Mansor, A.A., Napi, N.N.L.M., Mansor, W.N.W., Ahmed, A.N., Ismail, M., Ramly, Z.T.A., 2020. Air quality status during 2020 Malaysia Movement Control Order (MCO) due to 2019 novel coronavirus (2019-nCoV) pandemic. Sci. Total Environ. 729, 139022.

Agarwal, A., Kaushik, A., Kumar, S., Mishra, R.K., 2020. Comparative study on air quality status in Indian and Chinese cities before and during the COVID-19 lockdown period. Air Qual. Atmos. Health 13 (10), 1167–1178.

Ali, G., Abbas, S., Qamer, F.M., Wong, M.S., Rasul, G., Irteza, S.M., Shahzad, N., 2021. Environmental impacts of shifts in energy, emissions, and urban heat island during the COVID-19 lockdown across Pakistan. J. Clean. Prod. 291, 125806.

Alqasemi, A.S., Hereher, M.E., Kaplan, G., Al-Quraishi, A.M.F., Saibi, H., 2021. Impact of COVID-19 lockdown upon the air quality and surface urban heat island intensity over the United Arab Emirates. Sci. Total Environ. 767, 144330.

Arnfield, A.J., 2003. Two decades of urban climate research: a review of turbulence, exchanges of energy and water, and the urban heat island. Int. J. Climatol. 23 (1), 1–26.

Ayanlade, A., Atai, G., Jegede, M.O., 2019. Variability in atmospheric aerosols and effects of humidity, wind and InterTropical discontinuity over different ecological zones in Nigeria. Atmos. Environ. 201, 369–380.

Bauwens, M., Compernolle, S., Stavrakou, T., Müller, J.-F., van Gent, J., Eskes, H., Levelt, P.F., van der A., R., Veefkind, J.P., Vlietinck, J., Yu, H., Zehner, C., 2020. Impact of coronavirus outbreak on NO2 pollution assessed using TROPOMI and OMI observations. Geophys. Res. Lett. 47 (11) e2020GL087978.

Bekbulat, B., Apte, J.S., Millet, D.B., Robinson, A.L., Wells, K.C., Presto, A.A., Marshall, J.D., 2021. Changes in criteria air pollution levels in the US before, during, and after Covid-19 stay-at-home orders: evidence from regulatory monitors. Sci. Total Environ. 769, 144693.

Benali, A., Carvalho, A.C., Nunes, J.P., Carvalhais, N., Santos, A., 2012. Estimating air surface temperature in Portugal using MODIS LST data. Remote Sens. Environ. 124 (none), 108–121.

Benchrif, A., Wheida, A., Tahri, M., Shubbar, R.M., Biswas, B., 2021. Air quality during three covid-19 lockdown phases: AQI, PM2.5 and NO2 assessment in cities with more than 1 million inhabitants. Sustain. Cities Soc. 74, 103170.

Cai, Z., Tang, Y., Zhan, Q., 2021. A cooled city? Comparing human activity changes on the impact of urban thermal environment before and after city-wide lockdown. Build. Environ. 195, 107729.

Cao, X., Liu, X., Hadiatullah, H., Xu, Y., Zhang, X., Cyrys, J., Zimmermann, R., Adam, T., 2022. Investigation of COVID-19-related lockdowns on the air pollution changes in Augsburg in 2020, Germany. Atmos. Pollut. Res. 13 (9), 101536.

Chakraborty, T., Lee, X., 2019. A simplified urban-extent algorithm to characterize surface urban heat islands on a global scale and examine vegetation control on their spatiotemporal variability. Int. J. Appl. Earth Obs. Geoinf. 74, 269–280.

Chakraborty, T., Sarangi, C., Lee, X., 2021. Reduction in human activity can enhance the urban heat island: insights from the COVID-19 lockdown. Environ. Res. Lett. 16.

Chen, Y., Zhang, S., Peng, C., Shi, G., Tian, M., Huang, R.-J., Guo, D., Wang, H., Yao, X., Yang, F., 2020. Impact of the COVID-19 pandemic and control measures on air quality and aerosol light absorption in Southwestern China. Sci. Total Environ. 749, 141419.

Chu, D., 2006. Analysis of the Relationship Between MODIS Aerosol Optical Depth and PM (2.5) in the Summertime US.

Cugerone, K., De Michele, C., Ghezzi, A., Gianelle, V., 2018. Aerosol removal due to precipitation and wind forcings in Milan urban area. J. Hydrol. 556, 1256–1262.

Deng, M., Lai, G., Li, Q., Li, W., Pan, Y., Li, K., 2022. Impact analysis of COVID-19 pandemic control measures on nighttime light and air quality in cities. Remote Sens. Appl.: Soc. Environ. 27, 100806.

Didan, K., 2015. MOD13A2 MODIS/Terra Vegetation Indices 16-Day L3 Global 1km SIN Grid V006 [Data set]. NASA EOSDIS Land Processes DAAC. Accessed 2022-10-06 from https://doi.org/10.5067/MODIS/MOD13A2.006.

Du, H., Wang, D., Wang, Y., Zhao, X., Qin, F., Jiang, H., Cai, Y., 2016. Influences of land cover types, meteorological conditions, anthropogenic heat and urban area on surface urban heat island in the Yangtze River Delta Urban Agglomeration. Sci. Total Environ. 571, 461–470.

El Kenawy, A.M., Lopez-Moreno, J.I., McCabe, M.F., Domínguez-Castro, F., Peña-Angulo, D., Gaber, I.M., Alqasemi, A.S., Al Kindi, K.M., Al-Awadhi, T., Hereher, M.E., Robaa, S.M., Al Nasiri, N., Vicente-Serrano, S.M., 2021. The impact of COVID-19 lockdowns on surface urban heat island changes and air-quality improvements across 21 major cities in the Middle East. Environ. Pollut. 288, 117802.

Elvidge, C.D., Baugh, K.E., Zhizhin, M., Hsu, F.-C., 2013. Why VIIRS data are superior to DMSP for mapping nighttime lights. Proc. Asia-Pac. Adv. Netw. 35 (0), 62.

Elvidge, C.D., Baugh, K., Zhizhin, M., Hsu, F.C., Ghosh, T., 2017. VIIRS night-time lights. Int. J. Remote Sens. 38 (21), 5860–5879.

Fiedler, S., Wyser, K., Rogelj, J., van Noije, T., 2021. Radiative effects of reduced aerosol emissions during the COVID-19 pandemic and the future recovery. Atmos. Res. 264, 105866.

Hidalgo García, D., Arco Díaz, J., 2022. Impacts of the COVID-19 confinement on air quality, the land surface temperature and the urban heat island in eight cities of Andalusia (Spain). Remote Sens. Appl.: Soc. Environ. 25, 100667.

Hu, M., Chen, Z., Cui, H., Wang, T., Zhang, C., Yun, K., 2021. Air pollution and critical air pollutant assessment during and after COVID-19 lockdowns: evidence from pandemic hotspots in China, the Republic of Korea, Japan, and India. Atmos. Pollut. Res. 12 (2), 316–329.

Jamei, E., Jamei, Y., Seyedmahmoudian, M., Horan, B., Mekhilef, S., Stojcevski, A., 2022. Investigating the impacts of COVID-19 lockdown on air quality, surface Urban Heat Island, air temperature and lighting energy consumption in City of Melbourne. Energy Strategy Rev. 44, 100963.

Jin, M., Shepherd, M., Zheng, W., 2010. Urban surface temperature reduction via the urban aerosol direct effect: a remote sensing and WRF model sensitivity study. Adv. Meteorol. 2010.

Jing, W., Yang, Y., Yue, X., Zhao, X., 2016. A spatial downscaling algorithm for satellite-based precipitation over the Tibetan plateau based on NDVI, DEM, and land surface temperature. Remote Sens. 8 (8), 655.

Kovács, K.D., 2022. Determination of the human impact on the drop in NO2 air pollution due to total COVID-19 lockdown using Human-Influenced Air Pollution Decrease Index (HIAPDI). Environ. Pollut. 306, 119441.

Lal, P., Kumar, A., Kumar, S., Kumari, S., Saikia, P., Dayanandan, A., Adhikari, D., Khan, M.L., 2020. The dark cloud with a silver lining: assessing the impact of the SARS COVID-19 pandemic on the global environment. Sci. Total Environ. 732, 139297.

Li, L., Li, Q., Huang, L., Wang, Q., Zhu, A., Xu, J., Liu, Z., Li, H., Shi, L., Li, R., Azari, M., Wang, Y., Zhang, X., Liu, Z., Zhu, Y., Zhang, K., Xue, S., Ooi, M.C.G., Zhang, D., Chan, A., 2020. Air quality changes during the COVID-19 lockdown over the Yangtze River Delta Region: an insight into the impact of human activity pattern changes on air pollution variation. Sci. Total Environ. 732, 139282.

Lin, Y., Zhang, Y., Xie, F., Fan, M., Liu, X., 2021. Substantial decreases of light absorption, concentrations and relative contributions of fossil fuel to light-absorbing carbonaceous aerosols attributed to the COVID-19 lockdown in east China. Environ. Pollut. 275, 116615.
Liu, Z., Lai, J., Zhan, W., Bechtel, B., Voogt, J., Quan, J., Hu, L., Fu, P., Huang, F., Li, L., Guo, Z., Li, J., 2022. Urban heat islands significantly reduced by COVID-19 lockdown. Geophys. Res. Lett. 49 (2) e2021GL096842.
Lyapustin, A., Wang, Y., 2018. MCD19A2 MODIS/Terra + Aqua Land Aerosol Optical Depth Daily L2G Global 1km SIN Grid V006 [Data set]. NASA EOSDIS Land Processes DAAC. Accessed 2022-10-06 from https://doi.org/10.5067/MODIS/MCD19A2.006.
Mandal, J., Chanda, A., Samanta, S., 2022. Air pollution in three megacities of India during the Diwali festival amidst COVID-19 pandemic. Sustain. Cities Soc. 76, 103504.
Martinez-Soto, A., Avendaño Vera, C.C., Boso, A., Hofflinger, A., Shupler, M., 2021. Energy poverty influences urban outdoor air pollution levels during COVID-19 lockdown in south-central Chile. Energy Policy 158, 112571.
Mousazadeh, M., Paital, B., Naghdali, Z., Mortezania, Z., Hashemi, M., Karamati Niaragh, E., Aghababaei, M., Ghorbankhani, M., Lichtfouse, E., Sillanpää, M., Hashim, K.S., Emamjomeh, M.M., 2021. Positive environmental effects of the coronavirus 2020 episode: a review. Environ. Dev. Sustain. 23 (9), 12738–12760.
Neff, J.C., Reynolds, R.L., Munson, S.M., Fernandez, D., Belnap, J., 2013. The role of dust storms in total atmospheric particle concentrations at two sites in the western U.S. J. Geophys. Res. Atmos. 118 (19), 11,201–211,212.
Oke, T., 1973. City size and the urban heat island. Atmos. Environ. 7, 769–779.
Oke, T.R., Mills, G., Christen, A., Voogt, J.A., 2017. Urban Climates. Cambridge University Press.
Pal, S.C., Chowdhuri, I., Saha, A., Ghosh, M., Roy, P., Das, B., Chakrabortty, R., Shit, M., 2022. COVID-19 strict lockdown impact on urban air quality and atmospheric temperature in four megacities of India. Geosci. Front. 101368.
Parida, B.R., Bar, S., Kaskaoutis, D., Pandey, A.C., Polade, S.D., Goswami, S., 2021a. Impact of COVID-19 induced lockdown on land surface temperature, aerosol, and urban heat in Europe and North America. Sustain. Cities Soc. 75, 103336.
Parida, B.R., Bar, S., Roberts, G., Mandal, S.P., Pandey, A.C., Kumar, M., Dash, J., 2021b. Improvement in air quality and its impact on land surface temperature in major urban areas across India during the first lockdown of the pandemic. Environ. Res. 199, 111280.
Peng, S., Piao, S., Ciais, P., Friedlingstein, P., Ottle, C., Breon, F.-M., Nan, H., Zhou, L., Myneni, R., 2011. Surface urban heat island across 419 global big cities. Environ. Sci. Technol. 46, 696–703.
Peng, S., Ding, Y., Liu, W., Li, Z., 2019. 1 km monthly temperature and precipitation dataset for China from 1901 to 2017. Earth Syst. Sci. Data 11 (4), 1931–1946.
Purwanto, P., Astuti, I.S., Rohman, F., Utomo, K.S.B., Aldianto, Y.E., 2022. Assessment of the dynamics of urban surface temperatures and air pollution related to COVID-19 in a densely populated City environment in East Java. Ecol. Inform. 71, 101809.
Qian, J., Meng, Q., Zhang, L., Hu, D., Hu, X., Liu, W., 2022. Improved anthropogenic heat flux model for fine spatiotemporal information in Southeast China. Environ. Pollut. 299, 118917.
Roshan, G., Sarli, R., Grab, S.W., 2021. The case of Tehran's urban heat island, Iran: impacts of urban 'lockdown' associated with the COVID-19 pandemic. Sustain. Cities Soc. 75, 103263.
Shikwambana, L., Kganyago, M., Mhangara, P., 2021. Temporal analysis of changes in anthropogenic emissions and urban heat islands during COVID-19 restrictions in Gauteng Province, South Africa. Aerosol Air Qual. Res. 21 (9), 200437.
Shulla, K., Voigt, B.-F., Cibian, S., Scandone, G., Martinez, E., Nelkovski, F., Salehi, P., 2021. Effects of COVID-19 on the Sustainable Development Goals (SDGs). Discov. Sustain. 2 (1), 15.
Sobrino, J.A., Jiménez-Muñoz, J.C., Sòria, G., Romaguera, M., Guanter, L., Moreno, J., Plaza, A., Martínez, P., 2008. Land surface emissivity retrieval from different VNIR and TIR sensors. IEEE Trans. Geosci. Remote Sens. 46 (2), 316–327.
Toro, A.R., Catalán, F., Urdanivia, F.R., Rojas, J.P., Manzano, C.A., Seguel, R., Gallardo, L., Osses, M., Pantoja, N., Leiva-Guzman, M.A., 2021. Air pollution and COVID-19 lockdown in a large South American city: Santiago Metropolitan Area, Chile. Urban Clim. 36, 100803.
Tyagi, B., Choudhury, G., Vissa, N.K., Singh, J., Tesche, M., 2021. Changing air pollution scenario during COVID-19: redefining the hotspot regions over India. Environ. Pollut. 271, 116354.
Voogt, J.A., Oke, T.R., 2003. Thermal remote sensing of urban climates. Remote Sens. Environ. 86 (3), 370–384.
Wan, Z., 2008. New refinements and validation of the MODIS land-surface temperature/emissivity products. Remote Sens. Environ. 112 (1), 59–74.
Wan, Z., Hook, S., Hulley, G., 2021. MODIS/Aqua Land Surface Temperature/Emissivity Daily L3 Global 1km SIN Grid V061 [Data set]. NASA EOSDIS Land Processes DAAC. Accessed 2022-10-06 from https://doi.org/10.5067/MODIS/MYD11A1.061.
Wang, J., Huang, B., Fu, D., Atkinson, P.M., Zhang, X., 2016. Response of urban heat island to future urban expansion over the Beijing–Tianjin–Hebei metropolitan area. Appl. Geogr. 70 (70), 26–36.
Wang, Q., Su, M., 2020. A preliminary assessment of the impact of COVID-19 on environment – a case study of China. Sci. Total Environ. 728, 138915.
Wei, J., Li, Z., Lyapustin, A., Sun, L., Peng, Y., Xue, W., Su, T., Cribb, M., 2021. Reconstructing 1-km-resolution high-quality PM2.5 data records from 2000 to 2018 in China: spatiotemporal variations and policy implications. Remote Sens. Environ. 252, 112136.
WHO, 2020. Weekly Epidemiological Update on COVID-19 - 30 November 2022. Accessed 2022-12-02 from: https://www.who.int/publications/m/item/weekly-epidemiological-update-on-covid-19—30-november-2022.
WHO, 2022. Coronavirus Disease 2019 (COVID-19) Situation Report – 51. Accessed 2022-10-06 from https://www.who.int/docs/default-source/coronaviruse/situation-reports/20200311-sitrep-51-covid-19.pdf?sfvrsn=1ba62e57_10.
Wu, C., Wang, H., Cai, W., He, H., Ni, A., Peng, Z., 2021. Impact of the COVID-19 lockdown on roadside traffic-related air pollution in Shanghai, China. Build. Environ. 194, 107718.
Xiang, Y., Ye, Y., Peng, C., Teng, M., Zhou, Z., 2022. Seasonal variations for combined effects of landscape metrics on land surface temperature (LST) and aerosol optical depth (AOD). Ecol. Indic. 138, 108810.
Yang, M., Chen, L., Msigwa, G., Tang, K.H.D., Yap, P.-S., 2022a. Implications of COVID-19 on global environmental pollution and carbon emissions with strategies for sustainability in the COVID-19 era. Sci. Total Environ. 809, 151657.
Yang, X., Xiao, D., Fan, L., Li, F., Wang, W., Bai, H., Tang, J., 2022b. Spatiotemporal estimates of daily PM2.5 concentrations based on 1-km resolution MAIAC AOD in the Beijing–Tianjin–Hebei, China. Environ. Challenges 8, 100548.
You, W., Zang, Z., Zhang, L., Li, Z., Chen, D., Zhang, G., 2015. Estimating ground-level PM10 concentration in northwestern China using geographically weighted regression based on satellite AOD combined with CALIPSO and MODIS fire count. Remote Sens. Environ. 168, 276–285.
Zhao, N., Wang, G., Li, G., Lang, J., Zhang, H., 2020. Air pollution episodes during the COVID-19 outbreak in the Beijing–Tianjin–Hebei region of China: an insight into the transport pathways and source distribution. Environ. Pollut. 267, 115617.
Zhou, X., Strezov, V., Jiang, Y., Kan, T., Evans, T., 2022. Temporal and spatial variations of air pollution across China from 2015 to 2018. J. Environ. Sci. 112, 161–169.